

Ultrasonic Probing System with Multiple Transmitters and Multiple Receivers with Undersampling

Amoon Khalil* and Dmitry Y. Sukhanov

Abstract—Wave probing systems are used to obtain 2D or 3D images of objects. According to the nature of the waves used (acoustic — microwave and others), these waves can penetrate the fabrics or barriers that are in their way, so it is possible to photograph hidden objects. A system for ultrasonic wideband probing in air with multiple transmitters and multiple receivers with parallel digitization of signals from the receiving array using undersampling is proposed. Probing at frequencies from 38 kHz to 43 kHz is considered when receiving array signals are digitized at a frequency of 18 kHz. Transmitter and receiver placements have been optimized to minimize artifacts and noise. The transmitting and receiving arrays are located at the same plane. The presented results of the experimental study confirm that the processing of measured signals based on spatially matched filtering makes it possible to visualize scattering objects in the environment, including those hidden behind sound-permeable barriers.

1. INTRODUCTION

Imaging systems based on radio wave and acoustic fields are of great interest in many applications such as non-destructive testing, security scanning, medical diagnostics, and visualization of hidden objects through walls and tissues [1–12].

Fixed-aperture probing systems used in image processing systems based on reflectors and lenses make it possible to implement inexpensive devices with a compact design, but have a relatively low resolution and slow mechanical scanning [4, 5]. The aperture synthesis method is among the main methods of image reconstruction based on wave probing data [5].

Signal processing, for example, by the time domain migration method [8] or the Stolt method [9], makes it possible to obtain high-resolution three-dimensional images. In [4], a modified method based on Kirchhoff migration [13] was presented, used for systems with Multiple Transmitters and Multiple Receivers or Multiple Input and Multiple Output (MIMO) of the near field. It provides high computational efficiency through the application of the fast Fourier transform.

There are ultrasonic imaging methods used for nondestructive testing [1, 14–17]. According to [16], the most popular methods in this area are the full focusing method [14], inverse wavefield extrapolation [17], and the wavenumber algorithm [15]. It is believed that all these methods demonstrate the same performance in terms of resolution [14]. They can also be expressed as a linear superposition of transmitter-receiver signals in the frequency domain with different amplitudes and phases for each scatterer placement point [16].

Previously, a new approach, called the multistatic approach, was introduced, which was implemented through the sequential or simultaneous operation of spatially separated transmitting/receiving arrays or MIMO. The concept of MIMO is to use several emitters and several receivers sequentially or simultaneously [18, 19] to obtain various independent combinations

Received 29 August 2022, Accepted 1 November 2022, Scheduled 20 November 2022

* Corresponding author: Amoon Khalil (amoon.khalil16@gmail.com).

The authors are with the Tomsk State University, Tomsk, Russia.

(transmitter-scatterer-receiver paths) of the incident and scattered fields, which should provide information about the shape of the scattering object.

In this paper, we propose an implementation of an optimized MIMO system for ultrasonic probing in air with undersampling when digitizing the receiving signals. The optimization of the MIMO system was carried out for a point scatterer in the center of the aperture, minimizing the level of artifacts while maintaining the required resolution. Studies were carried out on the developed experimental setup with probing at frequencies from 38 to 43 kHz with a sampling frequency of 18 kHz.

2. FORWARD AND INVERSE PROBLEM

In the proposed probing system, linear frequency modulation (chirp) signals are used, which are classified as wideband signals. In this signal, the frequency changes linearly with time. This signal type was chosen for two main reasons. The first is physical and technical, since the energy of the chirp signal can be distributed over time and provide acceptable amplitudes for the linear mode of operation of the emitters and wave propagation. The second reason concerns mathematical signal processing, since the use of a wide bandwidth in imaging systems helps to reduce artifacts in the resulting image due to the incoherent response of artifacts at different frequencies.

The chirp signal can be written in the following form:

$$s(t) = A \sin \left(2\pi(t - t_s) \left[f_1 + \frac{(t - t_s)(f_2 - f_1)}{2(t_e - t_s)} \right] \right) \quad (1)$$

where A is the amplitude; t_s and t_e are the start and end times of the signal emission, respectively; f_1 is the initial frequency of the signal; f_2 is the end frequency of the signal. The current frequency of the signal is the derivative of its phase with respect to time.

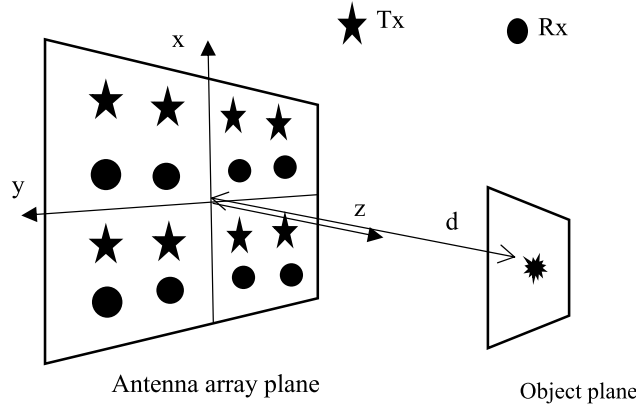


Figure 1. Geometry of the MIMO imaging system.

Consider a probing wideband signal, and suppose that the transmitting and receiving arrays are placed in the x - y plane, and the imaged object is located at a distance d from the array plane, as shown in Figure 1. Let the transmitters coordinates be given by a set of vectors \mathbf{T}_n , $n = 1 \dots N$, and the receivers coordinates be given by a set of vectors \mathbf{R}_m , $m = 1 \dots M$, where N and M are the numbers of transmitters and receivers, respectively. The forward problem of multistatic MIMO can be described as follows in the single scattering approximation [11]:

$$U(n, m, k) = A \iiint O(\mathbf{r}') S(\omega) \frac{\exp(ik(|\mathbf{T}_n - \mathbf{r}'| + |\mathbf{R}_m - \mathbf{r}'|))}{4\pi |\mathbf{T}_n - \mathbf{r}'| |\mathbf{R}_m - \mathbf{r}'|} d\mathbf{r}' \quad (2)$$

where $U(n, m, k)$ is the complex amplitude of the field in the m -th receiver during transmission of the n -th transmitter at a frequency $\omega = ck$; c is the speed of sound; k is the wave number; $|\mathbf{T}_n - \mathbf{r}'| = \sqrt{(x_n - x)^2 + (y_n - y)^2 + d^2}$ is the distance between the transmitter and the object under study; $|\mathbf{R}_m - \mathbf{r}'| = \sqrt{(x_m - x)^2 + (y_m - y)^2 + d^2}$ is the distance between the receiver and the object

under study; $O(\mathbf{r}')$ is a function describing the distribution of scattering inhomogeneities; $S(\omega)$ is the spectrum of the probing chirp signal.

The inverse problem or the process of reconstructing the image of an object can be solved mathematically by inverting the integration in Equation (2). This inversion can be applied using the deconvolution method with regularization. With a large regularization parameter, this method passes into the matched filtering method. Consider the method of matched filtering, where the signal from a point scatterer at a given point is considered as the detected signal. Then we write the reconstructed image in the form [19]:

$$\hat{O}(\mathbf{r}) = \sum_n \sum_m \sum_k U(n, m, k) S^*(\omega) \frac{\exp(-ik(|\mathbf{T}_n - \mathbf{r}| + |\mathbf{R}_m - \mathbf{r}|))}{|\mathbf{T}_n - \mathbf{r}| |\mathbf{R}_m - \mathbf{r}|} \quad (3)$$

where $S^*(\omega)$ is the complex conjugate spectrum of the probing signal.

Consider that the number of transmitting and receiving elements is 32 and 61, respectively. It is proposed to place both the transmitting and receiving elements in a hexagonal grid, with the same center and in the same plane. The step of the receiving array is 80 mm (much larger than the wavelength of 8 mm). Due to the sparsity of the receiving array, there may be artifacts. To reduce the level of artifacts, an optimization process should be carried out to select the transmitting array step and its rotation relative to the receiving array for a single point scatterer located at $\mathbf{r}_0 = (0, 0, d)$.

The image of a point scatterer $\hat{O}_0(\mathbf{r})$ can be written as follows:

$$\hat{O}_0(\mathbf{r}) = \sum_k P_s(\mathbf{r}, \omega) P_R(\mathbf{r}, \omega) \quad (4)$$

$$P_s(\mathbf{r}, \omega) = \sum_n \frac{\exp(ik(|\mathbf{T}_n - \mathbf{r}_0| - |\mathbf{T}_n - \mathbf{r}|))}{|\mathbf{T}_n - \mathbf{r}| |\mathbf{T}_n - \mathbf{r}_0|}, \quad P_R(\mathbf{r}, \omega) = \sum_m \frac{\exp(ik(|\mathbf{R}_m - \mathbf{r}_0| - |\mathbf{R}_m - \mathbf{r}|))}{|\mathbf{R}_m - \mathbf{r}| |\mathbf{R}_m - \mathbf{r}_0|}$$

where $P_s(\mathbf{r}, \omega)$ is the focused field of the transmitter array; $P_R(\mathbf{r}, \omega)$ is the focused field of the receiving array. The functions $P_s(\mathbf{r}, \omega)$ and $P_R(\mathbf{r}, \omega)$ were calculated for a frequency of 40 kHz, the speed of sound in air of 340 m/s for a scatterer placed opposite to the center of the aperture at a distance of 40 cm.

As a result of the optimization process, the transmitting array step was 12 mm, and its rotation angle relative to the receiving array was 90° (Figure 2).

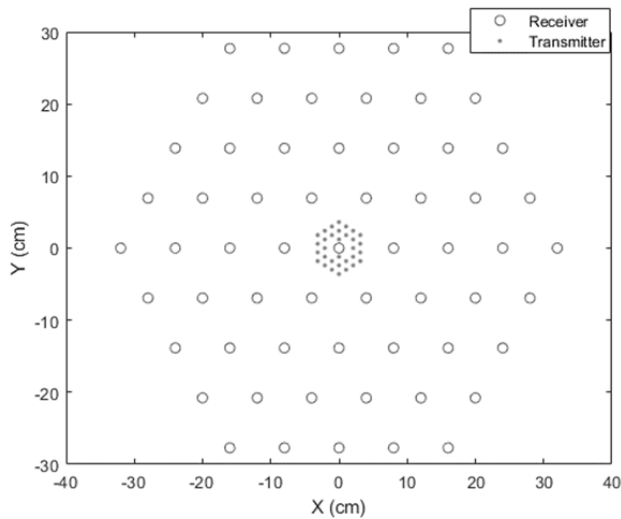


Figure 2. Placement of transmitters and receivers on a plane.

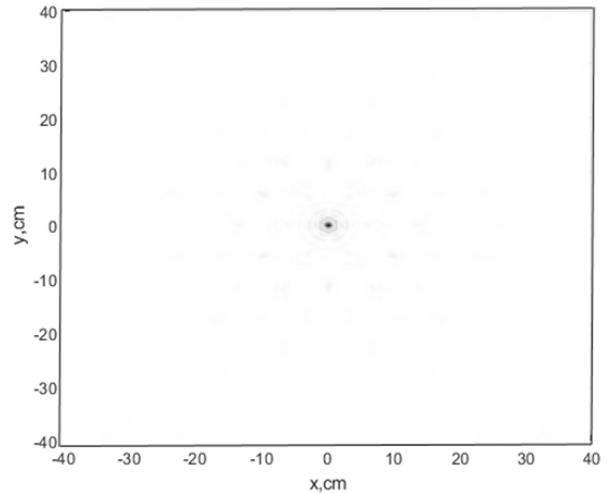


Figure 3. Point scatterer image at a distance of 40 cm using a wideband signal of a 38–43 kHz.

Figure 3 shows the image of point scatterer at a distance of 40 cm after optimization process when Formula (4) is applied using a 38–43 kHz wideband signal. The level of artifacts in this image is as minimal as possible for our system.

3. EXPERIMENTAL STUDIES

The experimental setup was developed based on the STM32F407 microcontroller (Figure 4). The microcontroller using two digital-to-analog converters (DAC) with a sampling rate of 578 kHz, and fed to 32 emitters through two 16-channel 74HC4067 multiplexers and LM837 amplifier, generates probing signals. The sampling frequency of the DAC is more than 13 times higher than the sweep frequency of the probing chirp signal (38–43 kHz) to minimize distortion of its shape and optimize the operation of ultrasonic emitter; at a lower sampling frequency, it is possible to generate sound waves in the audible range. The specific value of the frequency is chosen for reasons of synchronization with the receiving system of multiplexing and digitization. Each emitter is connected to a separate amplifier, and the 32 transmission channels are turned on in turn, so that only one emitter is working at a time. The emitters is placed in a hexagonal flat grating with a pitch of 12 mm.

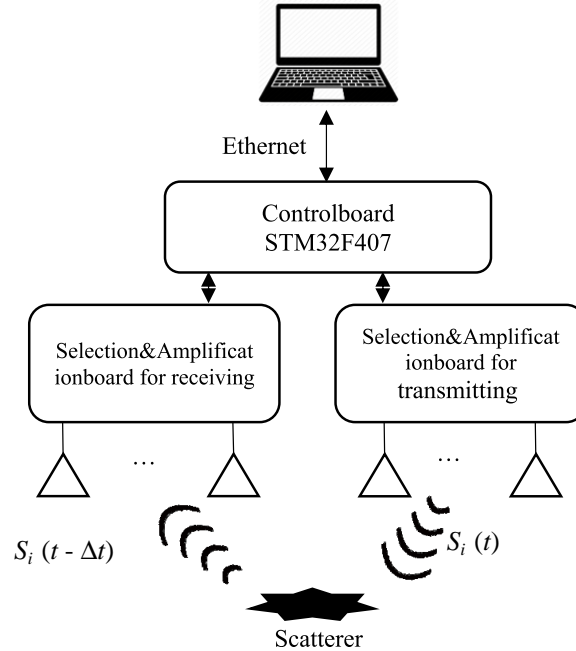


Figure 4. Connection diagram for emitters and receivers for signal digitization.

On the other hand, the receiving part consists of 61 receivers located in a hexagonal array in the same plane as the transmitting array; they have the same center, but they are rotated by 90 degrees (Figure 5). Received signals are amplified by an LMC6482A IC amplification circuit connected to each receiver. Receiving channels of 16 pieces are combined into one channel through a multiplexer, so 61 channels are converted into 4 channels when using 4×16 -channel multiplexers, then the output of these channels is connected to the inputs of four channels of analog-to-digital converters in the microcontroller. Due to the fast switching of multiplexers, almost simultaneous measurement of signals from all receivers is realized, and at the same time, a method of signal undersampling is realized. As a result, the digitization of signals for each channel is carried out individually at a frequency of 18 kHz, and the probing is carried out by a chirp signal in the frequency range from 38 kHz to 43 kHz. After subsampled digitization, this frequency range is observed as 2–7 kHz, which was taken into account in signal processing.

Digital data is transferred from the microcontroller to the computer for signal processing via the Ethernet interface using the UDP protocol. Due to parallel digitization from the receiving array and continuous data transmission, the system provides 4.4 frames per second.

Three experiments were carried out to visualize a plastic object in the shape of a gun. We assume that the distance between the object and the array is not exactly known in advance, but it can be determined from the delay of the reflected signal. In the first experiment, the object was located at a

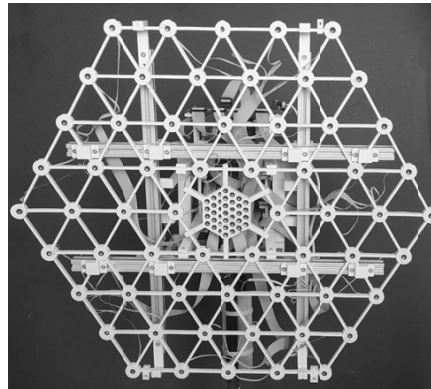


Figure 5. Photograph of the experimental setup of 61 receivers and 32 emitters.

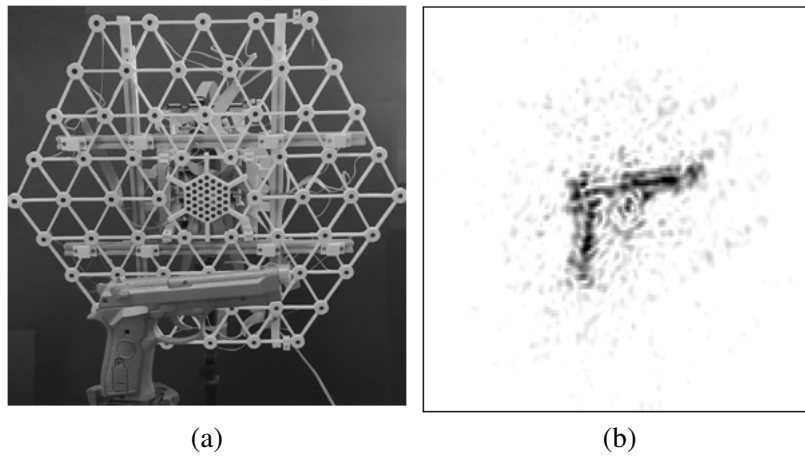


Figure 6. Photograph of the experiment on ultrasonic probing of a gun shape object.

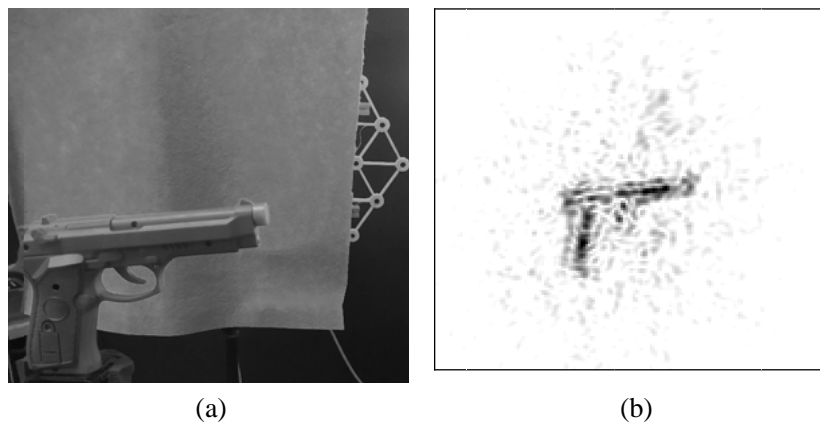


Figure 7. Photograph of the experiment on ultrasonic probing of a secret object, with plain fabric between the array and the object.

distance of 40 cm from the plane of the antenna array (Figure 6(a)), where the reconstructed image shows artifacts and noise (Figure 6(b)) caused by a sparse spatial distribution of transmitters and receivers. In addition, there are deviations of the sensors from their theoretical positions, and a difference in the

characteristics of each channel of the emitter and receiver. The second experiment is almost identical to the previous one. But there is a sound-permeable barrier in the form of a non-woven fabric (2 mm thickness) between the object and the antenna array (Figure 7(a)). The reconstructed image is slightly distorted compared to the first experiment (Figure 7(b)). In the third experiment, the object is covered with a sound-permeable fabric and is in direct contact with it (Figure 8(a)). It can be seen that the reconstructed image is more distorted and contains more noise and artifacts than the second experiment (Figure 8(b)). This is due to the impossibility to provide spatial resolution by the distance between the barrier and the object, since the image of the object and the image of the plain fabric are mutually superimposed. It should be noted here that the time required for data acquisition, processing, and object image reconstruction is 1 second. The time of data processing and image reconstruction can be reduced when using supercomputers.

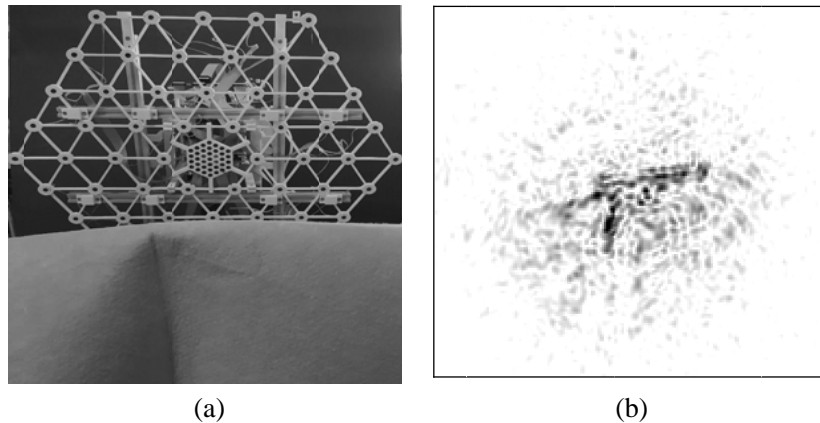


Figure 8. Photograph of the experiment on ultrasonic probing of a covered object which exist under a plain fabric.

4. CONCLUSION

A system for multistatic wideband ultrasonic probing in air based on a plurality of emitters (32) and a plurality of receivers (61) with digitization of signals with undersampling has been proposed. Transmitters and receivers are placed in a hexagonal array with different steps. The element spacing is optimized to minimize the level of artifacts while maintaining the specified spatial resolution. The system is controlled by the STM32F407 microcontroller and provides continuous data transmission via UDP protocol, which allows to achieve a refresh rate of 4.4 frames per second.

ACKNOWLEDGMENT

The work was supported by government task of Ministry of Science and Education of Russia, project N 0721-2020-0038.

REFERENCES

1. Velichko, A. and P. D. Wilcox, "An analytical comparison of ultrasonic array imaging algorithms," *J. Acoust. Soc. Am.*, Vol. 127, No. 4, 2377–2384, Apr. 2010, doi: 10.1121/1.3308470.
2. Samokrutov, A. A. and V. G. Shevaldykin, "Evaluation of defects in ultrasonic testing by digital focused array technique. The conditions, possibilities, boundaries of the applicability," *Diagnostic*, Vol. 9, 6–8, 2017, doi: 10.14489/td.2017.09.pp.006-018.
3. Wang, Q. H. and T. Ivanov, "Acoustic robot navigation using distributed microphone arrays," *Information Fusion*, Vol. 5, No. 2, 10, 2004, Art no. 2, doi: 10.1016/j.inffus.2003.10.002.

4. Zhuge, X. and A. G. Yarovoy, "Three-dimensional near-field MIMO array imaging using range migration techniques," *IEEE Trans. Image Process.*, Vol. 21, No. 6, 3026–3033, Jun. 2012, doi: 10.1109/TIP.2012.2188036.
5. Sheen, D. M., D. L. McMakin, and T. E. Hall, "Three-dimensional millimeter-wave imaging for concealed weapon detection," *IEEE Transactions on Microwave Theory and Techniques*, Vol. 49, No. 9, 9, 2001, doi: 10.1109/22.942570.
6. Pinchera, D., M. D. Migliore, F. Schettino, M. Lucido, and G. Panariello, "An effective compressed-sensing inspired deterministic algorithm for sparse array synthesis," *IEEE Transactions on Antennas and Propagation*, Vol. 66, No. 1, 11, 2018, doi: 10.1109/tap.2017.2767621.
7. Aboelyzeed, A. S. S., *Electronic Microwave Imaging with Planar Multistatic Arrays*, M-Logos-Verl, 2014.
8. Goldsmith, P. F., C. Hsieh, G. R. Huguenin, J. Kapitzky, and E. L. Moore, "Focal plane imaging systems for millimeter wavelengths," *IEEE Transactions on Microwave Theory and Techniques*, Vol. 41, No. 10, 12, 1993.
9. Stolt, R., "Migration by Fourier transform techniques," *Geophys.*, Vol. 43, 16, 1978.
10. Foorginejad, A., M. Taheri, and N. Mollayi, "A non-destructive ultrasonic testing approach for measurement and modelling of tensile strength in rubbers," *International Journal of Engineering*, Vol. 33, No. 12, 2549–2555, 2020, doi: 10.5829/ije.2020.33.12c.16.
11. Jamshidi, V. and R. Davarnejad, "Numerical analysis of backscatter radiography for prediction of pipelines situation: Their bursting and casing failure consideration from inside," *International Journal of Engineering*, Vol. 35, No. 2, 380–386, 2022, doi: 10.5829/ije.2022.35.02b.14.
12. Jamshidi, V. and R. Davarnejad, "Simulation of deposition detection inside wellbore by photon backscatter radiography," *International Journal of Engineering*, Vol. 33, No. 12, 2450–2454, 2020, doi: 10.5829/ije.2020.33.12c.03.
13. Zhuge, X., A. G. Yarovoy, T. G. Savelyev, and L. P. Lighthart, "Modified Kirchhoff migration for UWB MIMO array-based radar imaging," *IEEE Trans. Geosci. Remote Sens.*, Vol. 48, No. 6, 2692–2703, 2010.
14. Holmes, C., B. W. Drinkwater, and P. D. Wilcox, "Post-processing of the full matrix of ultrasonic transmit-receive array data for non-destructive evaluation," *NDT & E International*, Vol. 38, No. 8, 701–711, 2005, doi: 10.1016/j.ndteint.2005.04.002.
15. Hunter, A. J., B. W. Drinkwater, and P. D. Wilcox, "The wavenumber algorithm for full-matrix imaging using an ultrasonic array," *IEEE Transactions on Ultrasonics, Ferroelectrics and Frequency Control*, Vol. 55, No. 11, 2450–2462, 2008, doi: 10.1109/tuffc.952.
16. Zhang, J., B. W. Drinkwater, and P. D. Wilcox, "Comparison of ultrasonic array imaging algorithms for nondestructive evaluation," *IEEE Transactions on Ultrasonics, Ferroelectrics, and Frequency Control*, Vol. 60, No. 8, 1732–1745, 2013, doi: 10.1109/tuffc.2013.2754.
17. Portzgen, N., D. Gisolf, and G. Blacquiere, "Inverse wave field extrapolation: A different NDI approach to imaging defects," *IEEE Transactions on Ultrasonics, Ferroelectrics and Frequency Control*, Vol. 54, No. 1, 118–127, 2007, doi: 10.1109/tuffc.2007.217.
18. Liang, S., Z. Fang, G. Sun, Y. Liu, G. Qu, and Y. Zhang, "Sidelobe reductions of antenna arrays via an improved chicken swarm optimization approach," *IEEE Access*, Vol. 8, 37664–37683, 2020, doi: 10.1109/access.2020.2976127.
19. Sukhanov, D. Y. and M. A. Kalashnikova, "Remote ultrasonic defectoscopy of sound radiating objects through the air," *Acoust. Phys.*, Vol. 60, 304–308, 2014, <https://doi.org/10.1134/S1063771014030166>.